Delft University of Technology

Development of a Time–Height Profile Assimilation Technique for Large-Eddy Simulation

Allaerts, Dries; Quon, Eliot; Draxl, Caroline; Churchfield, Matthew

Important note
To cite this publication, please use the final published version (if applicable).
Please check the document version above.

Development of a Time–Height Profile Assimilation Technique for Large-Eddy Simulation

Dries Allaerts[1,2] · **Eliot Quon[2]** · **Caroline Draxl[2]** · **Matthew Churchfield[2]**

Abstract

Mesoscale-to-microscale coupling (MMC) aims to address the limited scope of traditional large-eddy simulations by driving the microscale flow with information concerning large-scale weather patterns provided by mesoscale models. We present a new offline MMC technique for horizontally homogeneous microscale flow conditions, in which internal forcing terms are computed based on mesoscale time–height profiles of mean-flow quantities. The advantage of such an approach is that it can be used to drive a microscale simulation with either mesoscale or observational data, and that it does not rely on specific terms in the mesoscale budget equations, which are typically not part of the default output of a mesoscale solver. The performance of the proposed profile assimilation technique is assessed based on the simulation of a typical diurnal cycle over the Scaled Wind Farm Technology site in west Texas. Results indicate that simple data assimilation techniques lead to unphysically high levels of shear and turbulence caused by the algorithm's inability to cope with inaccuracies in the mesoscale time–height profiles. Modifying the algorithm to account for vertical coherence in the mesoscale source terms gives the microscale solver a greater ability to correct the provided mesoscale time–height profiles, leading to improved predictions of shear and turbulence statistics. The resulting turbulence statistics are in good agreement with meteorological tower observations and simulation results obtained with state-of-the-art coupling techniques using mesoscale budget components.

Keywords Data assimilation · Diurnal cycle · Large-eddy simulation · Mesoscale-to-microscale coupling · Weather Research and Forecasting model

1 Introduction

For many years, large-eddy simulation (LES) models have provided a powerful tool to study microscale flow features in the atmosphere, such as boundary-layer processes, atmosphere–

✉ Eliot Quon
   eliot.quon@nrel.gov

1 Faculty of Aerospace Engineering, Delft University of Technology, Kluyverweg 1, 2629 HS Delft, The Netherlands

2 National Renewable Energy Laboratory (NREL), 15013 Denver West Parkway, Golden, CO 80401, USA

surface interactions, turbulence characteristics, and detailed terrain-induced flow patterns. However, the mesoscale meteorological phenomena that drive these microscale flows, such as frontal passages, thunderstorm outflows, atmospheric waves, and diurnal land–sea breezes, cannot be represented adequately in LES for two reasons. First, the LES technique for applications such as wind energy is specifically designed to resolve fine-scale flow features of tens to a single metre; as a result, the associated grid requirements, and hence computational requirements, restrict the domain size to the order of kilometres. Typical mesoscale phenomena, on the other hand, cover length scales ranging from 10 to more than 100 km, which cannot be represented on the limited microscale domain. Second, LES solvers focus mostly on flow dynamics and usually lack appropriate models to account for all the physical processes affecting mesoscale weather (e.g., radiation, microphysics, or land-surface models). Because of these limitations, the majority of fundamental and applied LES studies of the atmospheric boundary layer (ABL) reported to date have focused on idealized, canonical flow cases: the daytime buoyancy-driven boundary layer (e.g., Moeng 1984; Mason 1989; Nieuwstadt et al. 1993; Moeng and Sullivan 1994), the neutrally stratified ABL (e.g., Mason and Thomson 1987; Andren et al. 1994; Lin et al. 1996; Kosović 1997; Esau 2004; Pedersen et al. 2014), or the nocturnal stable boundary layer (e.g., Mason and Derbyshire 1990; Kosović and Curry 2000; Saiki et al. 2000; Beare et al. 2006; Basu and Porté-Agel 2006). Some recent works have applied four-dimensional data assimilation (Stauffer and Seaman 1994), or nudging, in LES to provide realistic forcing for convective (Gibbs et al. 2011) and stable (Gibbs and Fedorovich 2016) boundary layers; the former study considered large microscale grid spacings (100 m) and for both studies the forcing was applied with an hourly time scale. Only a handful of studies have performed LES of a full diurnal cycle (Duynkerke et al. 2004; Kumar et al. 2006, 2010; Kleissl et al. 2006; Basu et al. 2008). All of the diurnal-cycle studies, except Kumar et al. (2010), relied upon idealized forcing conditions and none of them accounted for large-scale advection of momentum or temperature.

Mesoscale-to-microscale coupling (MMC) aims to address the limited scope of traditional LES by driving microscale simulations with information concerning large-scale weather patterns provided by mesoscale models such as the Weather Research and Forecasting (WRF; Skamarock et al. 2008) model. The overall goal of MMC is to create a new predictive numerical simulation capability that is able to represent the full range of atmospheric flow conditions, to gain physical insights into complex fluid dynamics, and improve low-fidelity models and parametrizations. Applications of MMC are numerous and include urban meteorology (Baklanov and Nuterman 2009; Liu et al. 2012), pollutant dispersion (Nakayama et al. 2015), wildfire behaviour (Mandel et al. 2011), atmospheric two-phase flows such as snow transport (Vionnet et al. 2017), and wind-energy applications (Sanz Rodrigo et al. 2017a).

Although there are many ways to perform MMC, we focus on offline coupling of separate mesoscale and microscale solvers. Usually, offline coupling is achieved by prescribing mesoscale flow fields at the inflow boundaries of the microscale domain. As mesoscale solvers do not resolve microscale turbulence, flow perturbations or synthetic turbulence is superimposed on the mesoscale flow fields to accelerate the generation of turbulent structures (Mirocha et al. 2014; Muñoz-Esparza et al. 2015; Muñoz-Esparza and Kosović 2018; Quon et al. 2018). In relatively simple geographical and meteorological conditions, inflow turbulence generation can be avoided by using a laterally periodic microscale simulation, similar to idealized, canonical ABL simulations. The periodicity of the microscale domain allows a fully turbulent, horizontally homogeneous boundary layer to develop without the need for inflow perturbations or an intractably long upwind fetch. A key component of this approach is that information from the mesoscale simulation is transferred to the microscale simulation by applying horizontally homogeneous but time- and height-varying internal forcing terms

in the governing equations. This coupling approach is called an "internal forcing" technique. The assumption of horizontal homogeneity is valid in many situations, especially when the site of interest is in fairly flat terrain and when the horizontal heterogeneity is weak. This method can also be used to develop realistic turbulence that is superimposed onto flow fields representing horizontally heterogeneous conditions.

The most straightforward way to determine internal forcing terms is to extract relevant components that make up the mesoscale momentum and temperature transport equation budgets, including the background horizontal driving pressure gradient, large-scale advection, and subsidence terms, and apply these terms directly in the microscale governing equations. These terms are generally extracted from a mesoscale numerical weather prediction (NWP) code. We refer to this coupling technique as the "mesoscale budget components approach." The technique has been used successfully in a number of studies (Baas et al. 2010; Neggers et al. 2012; Schalkwijk et al. 2015; Heinze et al. 2017; Sanz Rodrigo et al. 2017b; Olsen 2018). However, there remains a number of open research questions related to this coupling technique. For example, terms in the mesoscale transport equation often contain small-scale, spatio-temporal variability, but there is no consensus on whether or not this variability is realistic or a numerical artifact, and, if so, how this small-scale information should be excluded from the internal forcing terms. In a companion paper by Draxl et al. (2020) (D2020), we evaluate the use of the mesoscale budget components approach to couple a mesoscale NWP solver with a dedicated microscale wind-power-plant LES solver. There, we address the open issue of small-scale variability observed in some of the mesoscale transport equation terms and the effect of filtering away that variability. Other concerns about this approach include the fact that the microscale solution is not guaranteed to follow the mesoscale solution over time (most of the aforementioned studies require additional nonphysical nudging forces to prevent excessive model drift), and the fact that the mesoscale description of advection is sensitive to the numerical resolution and physical parametrizations employed in the mesoscale simulation (Baas et al. 2010; Bosveld et al. 2014). Furthermore, transport equation terms are usually not standard output from mesoscale models, so the code must be modified to write these quantities.

The goal of this study is to develop an alternative internal forcing technique that uses actual mesoscale variables such as wind speed and temperature, instead of mesoscale-transport-equation budget components. The idea of the proposed method, which is akin to data assimilation, is to inform the microscale solver about the mesoscale time–height history of relevant flow variables and have the microscale solver use this information to estimate internal forcing terms as the solution progresses forward in time. These forcing terms should be designed such that the microscale mean solution follows the mesoscale time–height history in a defined area within the mesoscale simulation, while still resolving all the turbulence that results from the mesoscale internal and surface forcing. This approach has no risk of model drift in time, and the required data are readily available in the standard output of mesoscale solvers. Moreover, by avoiding the use of mesoscale-transport-equation budget components, this approach is better suited to driving microscale simulations based on observational data, from meteorological masts or remote sensing devices, for example.

Throughout this work, we consider the same test site, mesoscale dataset, and microscale solver as in D2020, which allows us to focus on the quality of the proposed MMC method and facilitates comparison with the more established internal forcing technique based on mesoscale transport equation terms. In Sect. 2, we describe two algorithms used to compute internal forcing terms based on mesoscale time–height profiles. Section 3 briefly summarizes the case study and model set-up. The results obtained with the proposed forcing-term

algorithms are then compared with the mesoscale budget components approach and with meteorological tower data in Sect. 4; conclusions are presented in Sect. 5.

2 Proposed Coupling Technique

2.1 Background

To understand the proposed coupling technique, we begin with the transport equations for momentum and virtual potential temperature that are solved by a typical microscale solver. The momentum equation, in incompressible form using the Boussinesq approximation for the buoyancy term, and the virtual potential temperature equation are

$$\frac{\partial \bar{u}_i}{\partial t} + \frac{\partial}{\partial x_j}\left(\bar{u}_i \bar{u}_j\right) + 2\epsilon_{ijk}\Omega_j\left(\bar{u}_k - u_k^G\right) = -\frac{1}{\rho_0}\frac{\partial \bar{p}'}{\partial x_i} - \frac{\partial \tau_{ij}^D}{x_j} + \left(\frac{\bar{\theta} - \theta_0}{\theta_0}\right)g_i, \quad (1a)$$

$$\frac{\partial \bar{\theta}}{\partial t} + \frac{\partial}{\partial x_j}\left(\bar{u}_j \bar{\theta}\right) = -\frac{\partial q_j}{\partial x_j}, \quad (1b)$$

where $\bar{u}_i$ is the resolved-scale velocity vector; ϵ_{ijk} is the alternating tensor indicating a cross product; Ω_j is the rotation rate vector of the system; u_k^G is the geostrophic wind vector; ρ_0 is the constant density; $\bar{p}'$ is the resolved-scale pressure perturbation away from: a reference value at a reference height, the hydrostatic variation with height (defined as $\rho_0 g_i x_i$), and the background mean horizontal gradient in pressure; τ_{ij}^D is the deviatoric part of the subgrid-scale stress tensor; $\bar{\theta}$ and θ_0 are the resolved-scale and reference virtual potential temperatures, respectively, that along with the gravity acceleration vector, g_i, comprise the Boussinesq buoyancy term; and q_j is the subgrid-scale temperature flux vector.

As an intermediate step in understanding the proposed technique, we next show how Eqs. 1a and 1b are modified in the "mesoscale budget components approach." This method is presented and analyzed in detail in the companion article by D2020, and later we show results from that method for comparison to the newly proposed assimilation technique. Modifications for the budget components approach are as follows,

$$\frac{\partial \bar{u}_i}{\partial t} + \frac{\partial}{\partial x_j}\left(\bar{u}_i \bar{u}_j\right) + 2\epsilon_{ijk}\Omega_j\bar{u}_k = S_{pg,i} + S_{adv,u_i} - \frac{1}{\rho_0}\frac{\partial \bar{p}'}{\partial x_i} - \frac{\partial \tau_{ij}^D}{x_j} + \left(\frac{\bar{\theta} - \theta_0}{\theta_0}\right)g_i, \quad (2a)$$

$$\frac{\partial \bar{\theta}}{\partial t} + \frac{\partial}{\partial x_j}\left(\bar{u}_j \bar{\theta}\right) = S_{adv,\theta} - \frac{\partial q_j}{\partial x_j}, \quad (2b)$$

where the S terms are time–height-varying source terms introduced into the microscale transport equations that arise from mesoscale-transport-equation budget components. $S_{pg,i} = S_{pg,i}(t, z)$ is the large-scale driving pressure gradient, $S_{adv,u_i} = S_{adv,u_i}(t, z)$ is the large-scale momentum advection term, and $S_{adv,\theta} = S_{adv,\theta}(t, z)$ is the large-scale virtual-potential-temperature advection term, all of which come from the mesoscale transport equations. Most commonly, these source terms are extracted from a mesoscale solver.

Equations 2a and 2b remain physics based because the microscale source terms correspond to physical terms from the mesoscale governing equations. They allow for a wider variety of flow situations than do the canonical situations that Eqs. 1a and 1b afford. The $S_{pg,i}$ term is a more arbitrary driving pressure gradient than that required to maintain a fixed geostrophic wind speed, and the S_{adv,u_i} and $S_{adv,\theta}$ terms allow the domain to realize bulk changes in

momentum and temperature from the large-scale advection of air masses into the domain while still maintaining a horizontally periodic framework.

2.2 The Proposed Data Assimilation Methods

Rather than using the physics-based time–height-varying source terms given from the mesoscale transport equation budgets, our proposed MMC technique aims to estimate these source terms as the microscale solution progresses forward in time given only information from the mesoscale time–height history of velocity and virtual potential temperature. The equations to be solved are

$$\frac{\partial \bar{u}_i}{\partial t} + \frac{\partial}{\partial x_j}\left(\bar{u}_i \bar{u}_j\right) + 2\epsilon_{ijk}\Omega_j \bar{u}_k = F_{u_i} - \frac{1}{\rho_0}\frac{\partial \bar{p}'}{\partial x_i} - \frac{\partial \tau_{ij}^D}{x_j} + \left(\frac{\bar{\theta}-\theta_0}{\theta_0}\right)g_i, \qquad (3a)$$

$$\frac{\partial \bar{\theta}}{\partial t} + \frac{\partial}{\partial x_j}\left(\bar{u}_j \bar{\theta}\right) = F_\theta - \frac{\partial q_j}{\partial x_j}. \qquad (3b)$$

Here, $F_{u_i} = F_{u_i}(t, z)$ is the forcing that aims to estimate the combined terms $S_{pg,i} + S_{adv,u_i}$ in Eq. 2a and $F_\theta = F_\theta(t, z)$ aims to estimate the $S_{adv,\theta}$ in Eq. 2b. The terms F_{u_i} and F_θ are estimated by some algorithm with the requirement that they drive the microscale planar-averaged solution toward the specified mesoscale time–height history.

From this point forward we use the following terminology: the word "source" refers to the physics-based terms extracted from the mesoscale governing equations that represent the synoptic driving pressure gradient and large-scale advection; the word "forcing" describes the terms computed by an engineering-based algorithm that seeks to estimate the physics-based "source" terms using limited information about the flow.

In the following discussion, we present two algorithms with which to compute the forcings F_{u_i} and F_θ. The first algorithm relies directly on data assimilation, or Newtonian relaxation, and is discussed in Sect. 2.2.1. The second algorithm accounts for vertical coherence in the source terms and is developed in Sect. 2.2.2.

2.2.1 Direct Data Assimilation

An intuitive approach to estimate time- and height-dependent mesoscale source terms takes the forcings to be proportional to the error $e_\varphi = \varphi_{\mathrm{meso}} - \langle\varphi\rangle$ between the mesoscale profile and the mean microscale profile, with φ representing the horizontal wind components u or v, or the virtual potential temperature, θ (moisture is not taken into account in the microscale simulation). The mean of the microscale result is computed by averaging over horizontal planes, denoted by the angle brackets, as the microscale flow is assumed to be horizontally homogeneous. The effect of the large-scale forcing enters the momentum and virtual potential temperature equations as

$$F_\varphi(t, z) = K_p e_\varphi(t, z) \qquad (4)$$

with $\varphi \in \{u, v, \theta\}$, where $K_p = 0.2 \text{ s}^{-1}$ is the controller gain. Equation 4 is evaluated at every vertical level and at every instant in time independently, which implies that the forcing term algorithm has no memory and the value of large-scale forcing at different vertical levels is uncorrelated.

The proposed algorithm is easy to implement in a microscale solver and ensures that the mean wind speed and virtual potential temperature follow the corresponding mesoscale
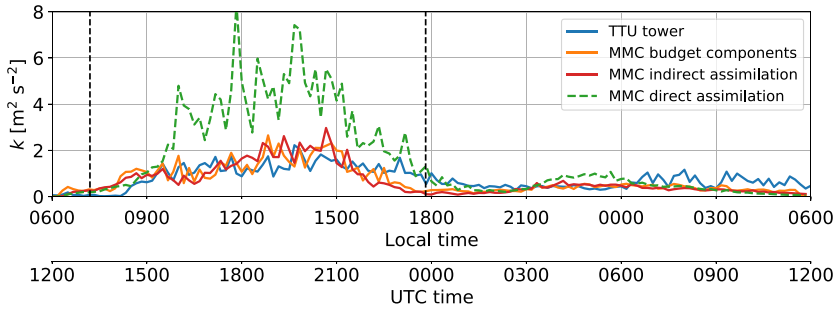
Fig. 1 Time history of TKE (k) for 8 and 9 November 2013 at a height of 80 m, comparing TTU tower observations with results obtained with direct data assimilation, indirect data assimilation, and budget components coupling. All results were computed with 10-min statistics from a single virtual tower in the microscale simulation. Vertical dashed black lines indicate sunrise and sunset

profiles. However, comparing the time history of turbulence kinetic energy (TKE, k) at 80 m with the Texas Tech University (TTU) tower observations in Fig. 1 shows that this approach strongly overpredicts the TKE during the daytime (other results shown in Fig. 1 are discussed in Sect. 4.3).

As will be explained in detail in Sect. 4, this algorithm fails because it does not account for possible errors in the mesoscale profiles and prohibits the microscale solver from altering the flow over microscale spatial and temporal scales. Therefore, a modified version of the algorithm, in which the variability of the calculated forcing terms is constrained by imposing vertical correlation, is proposed next.

2.2.2 Indirect Data Assimilation

The direct assimilation method is improved by correlating the controller actions at different vertical levels to one another by fitting a polynomial curve of order m to the vertical error profile $e_\varphi = \varphi_{\text{meso}} - \langle \varphi \rangle$, which introduces a form of vertical smoothing or low-pass filtering. We call this approach "indirect" data assimilation because the forcing terms depend only indirectly on the difference between the microscale flow solution and the reference profiles. The effect of the mesoscale sources then enters the governing equations as

$$F_\varphi(t, z) = K_p \tilde{e}_\varphi(t, z) \tag{5}$$

with $\varphi \in \{u, v, \theta\}$, where $\tilde{e}_\varphi = Z\hat{\beta}_\varphi$ is a polynomial fit of the error profile, e_φ. The vector of polynomial coefficients is denoted as $\hat{\beta}_\varphi = (\hat{\beta}_{\varphi,0}, \hat{\beta}_{\varphi,1}, \cdots \hat{\beta}_{\varphi,m})$, and

$$Z = \begin{bmatrix} 1 & z_1 & z_1^2 & \cdots & z_1^m \\ 1 & z_2 & z_2^2 & \cdots & z_2^m \\ \vdots & \vdots & \vdots & \ddots & \vdots \\ 1 & z_n & z_n^2 & \cdots & z_n^m \end{bmatrix}, \tag{6}$$

with $z_1, z_2, \ldots, z_n$ the vertical grid points. At every timestep, the polynomial coefficients are computed by minimizing the weighted sum of squares of the difference between the error profile and the polynomial fit,

$$\hat{\beta}_\varphi = \arg\min_\beta \| W^{1/2} \left(e_\varphi - Z\beta \right) \|_2^2, \tag{7}$$

with W a diagonal matrix of weights $w_k > 0$. Equation 7 is an unconstrained quadratic programming problem and is solved explicitly, giving

$$\hat{\beta}_\varphi = \left(Z^T W Z \right)^{-1} Z^T W e_\varphi. \tag{8}$$

By extending the direct data assimilation method with polynomial smoothing, the polynomial order, m, and distribution of weights, w_k, are introduced as additional controller parameters. The baseline configuration applies a cubic polynomial fit ($m = 3$) with uniform weight distribution for both momentum and virtual potential temperature forcing terms. As before, the controller gain is set to $K_p = 0.2 \text{ s}^{-1}$. Sensitivity to the various controller parameters will be addressed in Sect. 4.1.

3 Case Study and Model Set-up

We focus on MMC for relatively simple geographical and meteorological conditions. To this end, the U.S. Department of Energy's (DOE's) Scaled Wind Farm Technology (SWiFT) facility is selected as the site of interest. The SWiFT site is located in the southern Great Plains in Lubbock, Texas, with very minor terrain changes and no significant geographic features for hundreds of kilometres. The site is equipped with meteorological measurement facilities hosted by the National Wind Institute (NWI) at TTU, including a tall meteorological tower providing the three components of velocity, temperature, barometric pressure, and relative humidity measurements at 10 vertical levels, ranging from 0.9 to 200 m. Detailed information on the SWiFT site and NWI measurement facilities can be found in Hirth and Schroeder (2014) and Kelley and Ennis (2016).

MMC simulations of a complete diurnal cycle are used to assess the performance of the proposed internal forcing technique. Within the DOE's Atmosphere to Electrons (A2e) MMC project, meteorological conditions at the SWiFT site were analyzed for the period between 23 June 2012 and 31 December 2014 to identify a canonical diurnal cycle. The data were first searched for a consistent 1-h, near-neutral atmospheric stability condition and subsequently filtered—requiring that the surrounding 24 h have fairly consistent wind speed and wind direction—to remove cases with significant frontal passages. From the 36 days that satisfied this set of filter conditions, the evening transition on 8 November 2013 was selected because of its substantial diurnal forcing and relevance for wind-energy applications. During this day, conditions were generally clear and quiescent without precipitation. Stability was assessed using the bulk Richardson number, which ranged from −0.1 to 0.3 during the period of interest. Vertical gradients for the Richardson number are estimated from sonic anemometer measurements at 2.4 and 10.1 m above ground level. Details of the case selection procedure and a description of the meteorological conditions during the diurnal cycle on 8 November 2013 are given in Haupt et al. (2017).

The mesoscale conditions are computed using the WRF model, version 3.7.1. This simulation uses three nested domains centred at the SWiFT site with horizontal grid spacing of 27 km, 9 km, and 3 km, with the inner domain covering 354 km × 300 km. In the vertical direction, a total of 88 model levels are used with a spacing of 5 m in the lowest 20 m

and continuous stretching beyond that. The simulation is initialized on 8 November 2013 at 0000 UTC and advanced for 48 h, using a timestep of 15 s. All microscale simulations use mesoscale data from the data column nearest to the SWiFT site, with model output from the 3-km domain saved every 10 min.

The microscale flow is simulated with NREL's incompressible large-eddy simulation code, Simulator fOr Wind Farm Applications (SOWFA; see, e.g., Churchfield et al. 2012a, b), which is built upon the Open-source Field Operations And Manipulations (OpenFOAM) computational fluid dynamics toolbox. The code solves the conservation equations of mass, momentum, and virtual potential temperature (no moisture). We model a horizontally periodic domain of 5 km × 5 km × 2 km with a uniform grid spacing of 10 m in each direction, i.e., the grid cell aspect ratio is 1 everywhere within the domain. The microscale simulations are initialized on 8 November 2013 at 1200 UTC (corresponding to 0600 LT; local time = UTC − 6 h), using WRF profiles of velocity and virtual potential temperature, and the simulations are advanced for 24 h with a timestep of 0.5 s. All microscale simulations use the same boundary conditions: free-slip conditions and a fixed temperature gradient at the top and periodic boundary conditions at the sides. A standard wall-stress and heat-flux model (Schumann 1975; Grötzbach 1987) was applied at the bottom, with a uniform roughness length of 0.1 m. Surface virtual potential temperature from the WRF model along with the solved first-grid-level virtual potential temperature are used to compute a compatible surface heat flux using Monin–Obukhov scaling.

Further details regarding numerical discretization, physics schemes, and subgrid-scale modelling of both the mesoscale and the microscale solvers can be found in D2020.

4 Results and Discussion

Mesoscale-to-microscale simulations of the diurnal cycle on 8 November 2013 at the SWiFT site are performed using direct and indirect data assimilation, and using the mesoscale budget components approach (i.e., simulation *L3_T0* of D2020) for comparison. The results of these simulations are compared with observations from the TTU meteorological tower and WRF mesoscale data. First, the forcing terms computed by both the direct and indirect assimilation methods are assessed in Sect. 4.1, and the sensitivity of the indirect data assimilation algorithm to the various controller parameters is evaluated. Next, mean-flow results and turbulence statistics are analyzed in Sects. 4.2 and 4.3, respectively, and the overall performance and issues of the profile assimilation techniques are discussed in Sect. 4.4.

4.1 Computed Forcing Terms

The direct and indirect assimilation algorithms compute the time–height-varying forcing terms, F_{u_i} and F_θ, in Eqs. 3a and 3b. The objective of these terms is to estimate the physical source terms from the mesoscale governing equations that represent the pressure gradient force and large-scale advection of momentum and temperature. In other words, F_{u_i} estimates $S_{pg,i} + S_{adv,u_i}$ of Eq. 2a, and F_θ estimates $S_{adv,\theta}$ of Eq. 2b. In Fig. 2, we compare vertical profiles of F_{u_i} and F_θ from direct and indirect data assimilation with the physical source terms they seek to estimate. The mesoscale source terms were extracted from the 3-km WRF model domain at 10-min intervals. Results of indirect data assimilation, using both linear ($m = 1$) and cubic ($m = 3$) polynomials with uniform weighting, are included to show the effect of the polynomial order.
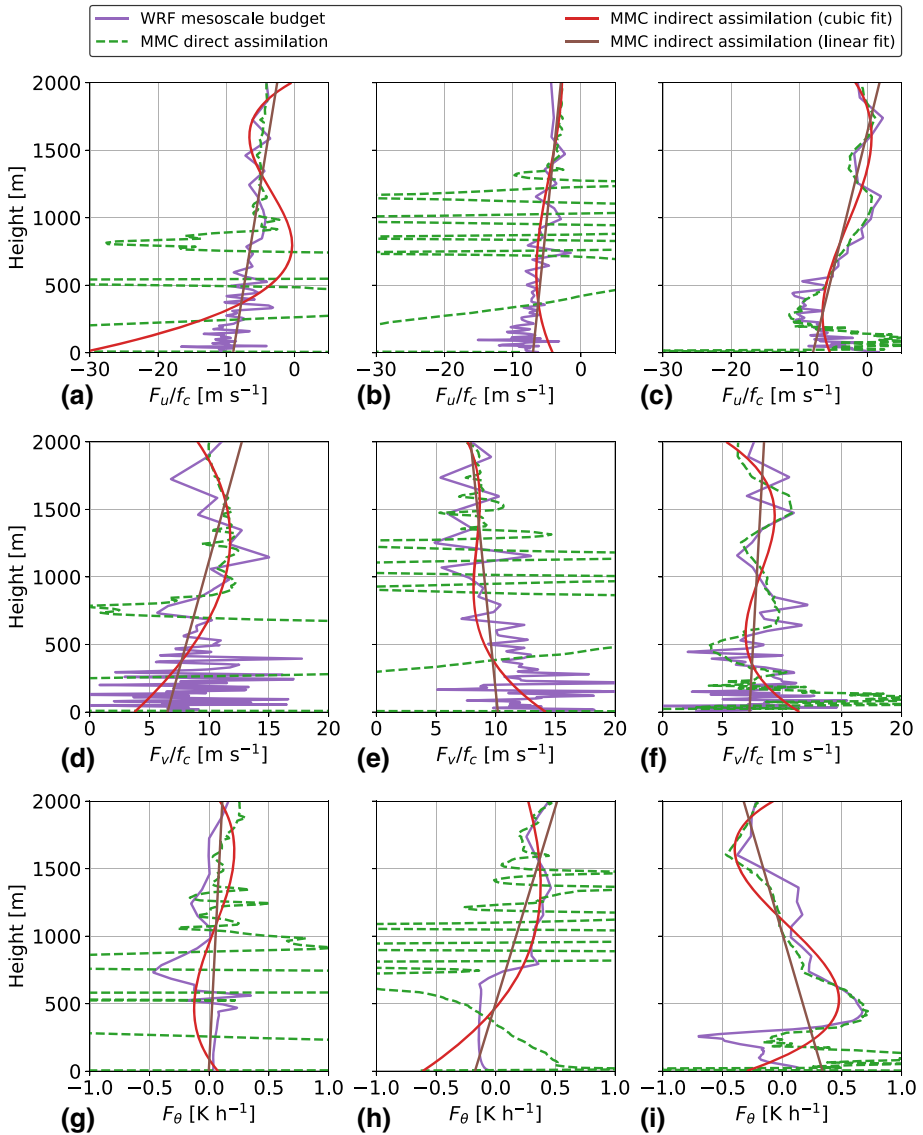
Fig. 2 Vertical profiles of data-assimilation-computed forcing terms for, **a–c** x-velocity component, **d–f** y-velocity component, and **g–i** virtual potential temperature, averaged over 1 h, starting at (left panel) 1800 UTC, (middle panel) 2200 UTC, and (right panel) 0600 UTC, for 8 and 9 November 2013. Forcing terms computed with direct and indirect data assimilation (using either cubic or linear fit with uniform weighting) are compared with mesoscale source terms extracted from the WRF mesoscale simulation. The momentum terms are scaled with the inverse of the Coriolis parameter, f_c. Note that for the WRF mesoscale budget, $F_{u_i} \equiv S_{pg,i} + S_{adv,u_i}$ and $F_\theta \equiv S_{adv,\theta}$

The vertical profiles have been averaged over one hour, starting on 8 November 2013 at 1800 UTC, 2200 UTC, and 0600 UTC, with the last time period occurring on the following day. These times correspond to 1200 LT, 1600 LT, and 0000 LT, respectively, and have been chosen to represent three different stability conditions characterized by the bulk Richardson number (Ri) and the Obukhov length (L). Whereas Ri is calculated from measurements at two heights, 2.4 and 10.1 m, L is calculated from 10-min statistics at 10.1 m alone. The period from 2200 to 2300 UTC corresponds to the 1-h, near-neutral period on the basis of which the diurnal cycle case was selected initially and is characterized by $Ri = -0.009$ and $L = -600$ m. We note that the near-neutral conditions here correspond to a transitional state between daytime and nighttime conditions—unlike canonical simulations of a stationary neutral ABL, this near-neutral state is not in equilibrium and has memory of the previous buoyancy-driven state. The other two periods are representative of the daytime convective ($Ri = -0.06$, $L = -100$ m) and night-time stable boundary layer ($Ri = 0.03$, $L = 200$ m).

The forcing-term profiles for both momentum and virtual potential temperature data assimilation show that indirect data assimilation predicts forcings of the correct order of magnitude. In most cases, the predicted vertical structure of the forcing also agrees well with the source terms extracted from the WRF model. Direct data assimilation, on the other hand, performs reasonably well above the boundary layer but overpredicts the amplitude of the source terms by several orders of magnitude within the boundary layer. Moreover, the profiles obtained with direct data assimilation are very noisy, due to lack of vertical correlation, whereas indirect data assimilation yields smoothly varying profiles, in accordance with the specified polynomial order.

Comparing forcing terms computed by indirect data assimilation shows that the cubic-fit approach, having greater degrees of freedom than the linear fit, enables prediction of more complex vertical structures. However, the higher polynomial order can also lead to a runaway near the edges of the profile (e.g., resulting in very large values near the surface in Fig. 2a and h). Higher-order polynomials will only exacerbate this problem, so we restrict our analysis to cubic-order polynomials or lower ($m \leq 3$). Further, we tested indirect data assimilation algorithms using non-uniform weight distributions, with lower weights below the boundary layer to express the fact that WRF predictions inside the boundary layer are more likely to be inaccurate, given the strong dependence on the ABL parametrization scheme. However, reducing weights near the surface aggravates the runaway effect even more and does not improve the simulation results (not shown).

Figure 3 shows time–height contours of the forcing term for mesoscale virtual-potential-temperature advection, computed with both direct and indirect data assimilation. For comparison, the mesoscale source term for virtual-potential-temperature advection, which the forcing term seeks to approximate, is also shown. The mesoscale forcing terms for momentum components are very similar for all the algorithms, therefore their time–height contours have not been shown. For reference, we have overlaid the height of the ABL, estimated as the height coinciding with the vertical heat-flux minima during convective conditions and the height at which the horizontal shear stresses are linearly extrapolated to zero (Kosović and Curry 2000) during stable conditions. The heat flux and shear stresses were calculated from planar-averaged statistics.

Indirect data assimilation with cubic fit (Fig. 3b) shows good qualitative agreement with the virtual-potential-temperature advection of the WRF model and is able to capture many of the large-scale spatial and temporal trends. For example, the algorithm predicts remarkably well the various patterns of cooling and heating between 1800 and 0000 LT that drive the microscale dynamics of the residual layer. During the daytime, the indirect assimilation with cubic fit also produces similar temperature forcing in the free atmosphere in terms
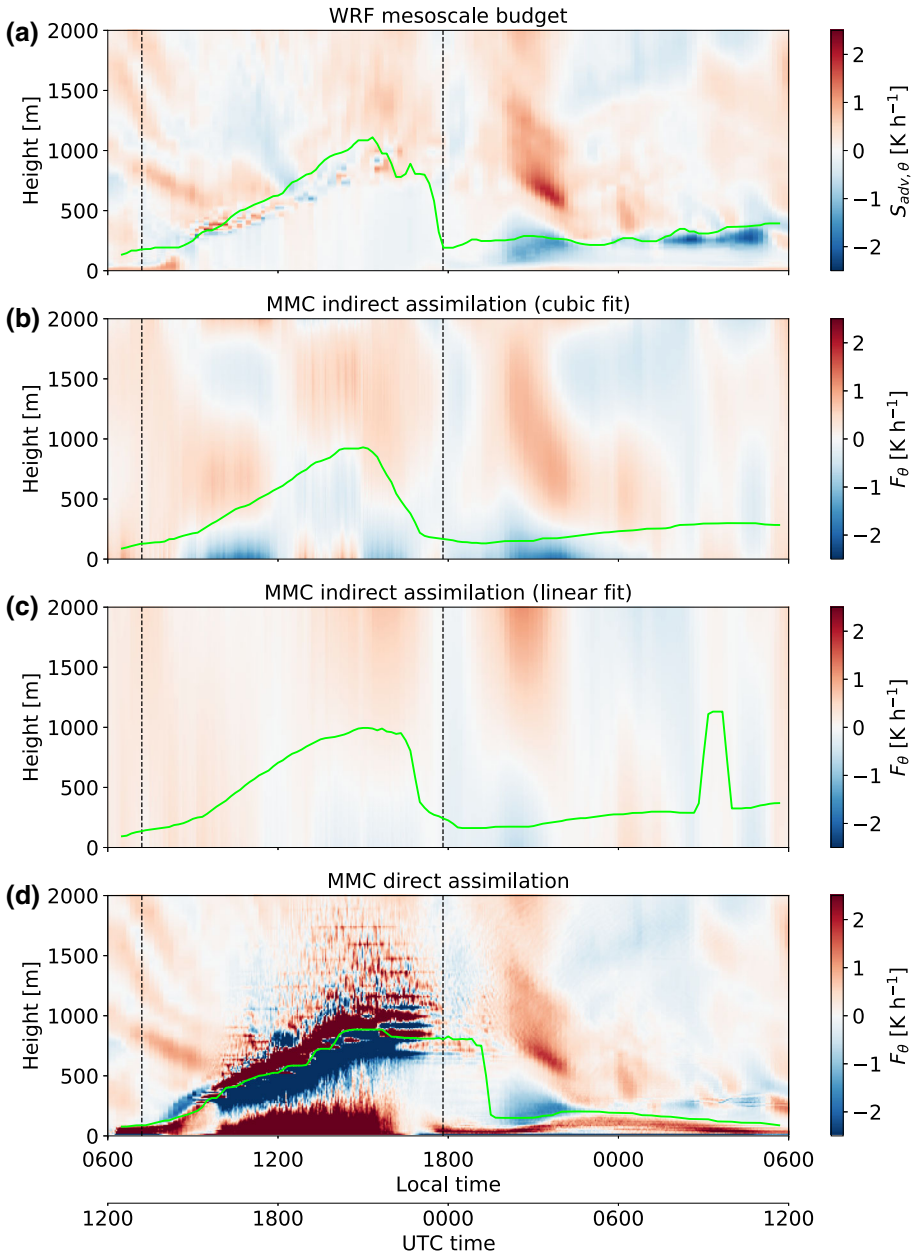
Fig. 3 Time–height profiles, between 8 and 9 November 2013, of the data-assimilation-computed forcing term for mesoscale virtual potential temperature advection. The forcings are computed with direct and indirect data assimilation (using either cubic or linear fit with uniform weighting), and they are compared with the mesoscale temperature advective term ($S_{adv,\theta}$) extracted from the WRF mesoscale simulation. The colour scale in **d** is clipped to ± 2.5 K h^{-1} to allow comparison with **a**–**c**, whereas the actual values obtained with direct data assimilation range from -87 to 33 K h^{-1}. The green curve shows the estimated boundary layer height and the vertical dashed black lines indicate sunrise and sunset

of magnitude and timing. The agreement between the linear fit in Fig. 3c and the WRF mesoscale model is not as good as the cubic fit, and some important cooling events during the transition from day to night are underpredicted, leading to an overprediction of the night-time boundary-layer temperature (not shown).

Figure 3d shows the large-scale virtual-potential-temperature advection predicted by direct data assimilation. At night, the forcing agrees reasonably well with the WRF model, although near the surface a strong heating event is predicted by direct data assimilation, contradicting the WRF mesoscale advective source and indirect data assimilation forcing, which are both close to zero. During the daytime, however, the simple algorithm yields very noisy forcing terms that are too large. While all forcing algorithms predict similar growth of the daytime convective mixed layer and agree that the ABL reaches a maximum height at around 1500 LT, the direct assimilation algorithm predicts a much later collapse of the daytime ABL.

In a preliminary test case, we tried applying a Gaussian filter in the vertical direction to the direct data assimilation result, but this approach still resulted in unrealistic microscale statistics. Further, we also tested the impact of the controller gain of the indirect data assimilation algorithm by running several simulations using a wide range of gain values, but we found no significant difference between the results for K_p ranging from 0.002 to 2 s^{-1}. Similarly, using a proportional-integral controller instead of a proportional controller in Eq. 5 did not alter the performance of the algorithm. We therefore conclude that the vertical smoothing (and hence the choice of polynomial order and weight distribution) dominates the dynamics of the algorithm, and we set the indirect data assimilation algorithm to use a non-weighted cubic fit with $K_p = 0.2$ s^{-1} in the remainder of the study.

4.2 Mean-Flow Quantities

Direct and indirect data assimilation predictions of the diurnal evolution of wind speed, wind direction, and virtual potential temperature at a height of 80 m are compared in Fig. 4. TTU tower observations, WRF mesoscale data, and results of the MMC budget components approach are included for reference. All microscale mean-flow quantities represent planar averages saved every 2.5 s, tower observations are 10-min temporally averaged, and WRF mesoscale data are obtained from the model column (3 km × 3 km cell) nearest the SWiFT site and saved every 10 min.

In terms of wind speed in Fig. 4a, simulations driven by direct and indirect data assimilation closely follow the mesoscale simulation and only agree with the observations when the mesoscale input data correctly predicts wind-speed evolution. Comparing direct and indirect data assimilation in more detail, we find that the former approach matches the mesoscale simulation almost exactly (the respective lines in Fig. 4a collapse onto each other most of the time), whereas the latter approach appears to be less restrictive and allows some deviations from the input profiles. By contrast, the budget components approach deviates significantly from the mesoscale simulation, because in this approach the wind speed results from the balance between large-scale forcing and microscale dynamics, and there is no additional nudging term to keep the microscale mean solution close to the mesoscale solution. In the current diurnal cycle, this microscale model drift in the budget components simulation leads to an improved agreement with observations, but, in general, this effect will not always be positive.

For wind direction and virtual potential temperature in Fig. 4b, c, direct data assimilation again follows the WRF mesoscale data very closely, and the results of MMC via indirect data assimilation and budget components evolve more freely about the mesoscale data. However,
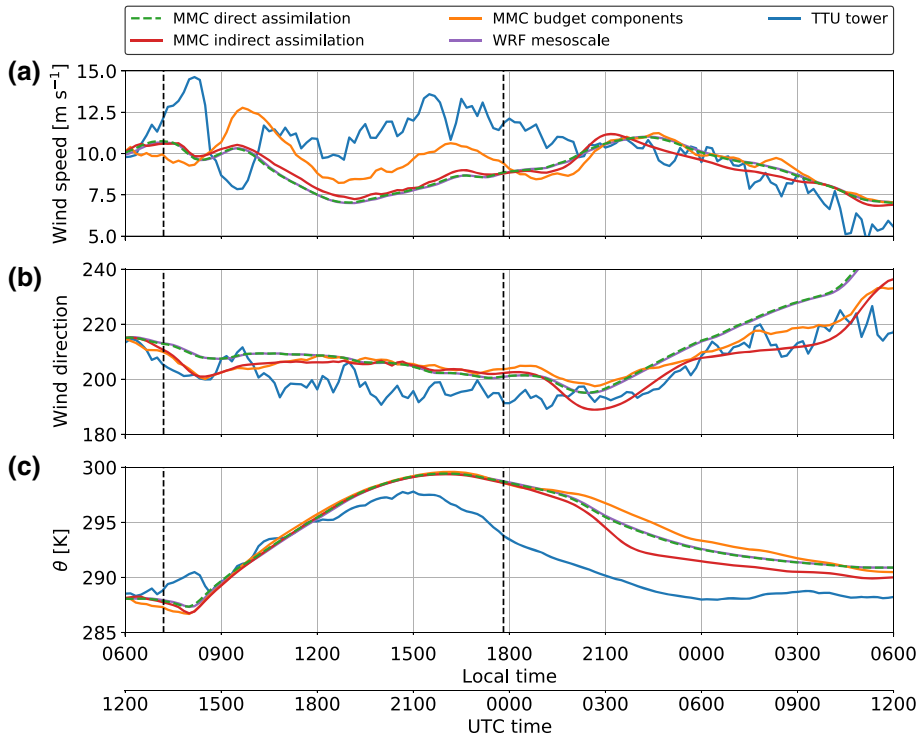
Fig. 4 Time history for 8 and 9 November 2013 at a height of 80 m of **a** horizontal wind speed, **b** wind direction, and **c** virtual potential temperature, comparing direct and indirect data assimilation with TTU tower observations, WRF mesoscale data, and MMC using budget components. The microscale results represent planar-averaged data. Vertical dashed black lines indicate sunrise and sunset

the agreement with observations again depends to a large extent on the mesoscale prediction, and this is particularly clear from the time history of the virtual potential temperature in Fig. 4c.

Insight into the vertical structure of the boundary layer throughout the diurnal cycle is provided in Fig. 5 in the form of vertical profiles of horizontal wind speed, wind direction, and virtual potential temperature at various times of the day (same times as in Fig. 2).

As before, the microscale mean-flow quantities are planar averaged, and the WRF mesoscale data are obtained from the model column nearest the SWiFT site.

The nearly perfect match between the forcing computed by direct data assimilation and the WRF mesoscale data also holds for the vertical structure of the boundary layer for all mean-flow quantities. Forcing from indirect data assimilation, on the other hand, deviates more from the mesoscale data, both within and above the boundary layer. Compared to the tower observations, the various MMC approaches underpredict wind speed during convective and neutral conditions, but the low-level jet during stable conditions is well captured by all microscale simulations. In terms of wind direction, the MMC approaches agree for convective and neutral, but not for stable conditions, and the indirect data assimilation approach overpredicts the wind veer in the lowest part of the boundary layer, compared to the observations. The high values of wind veer are attributed to runaway in the momentum forcing terms near the surface (see Fig. 2c, f and the discussion in Sect. 4.1).
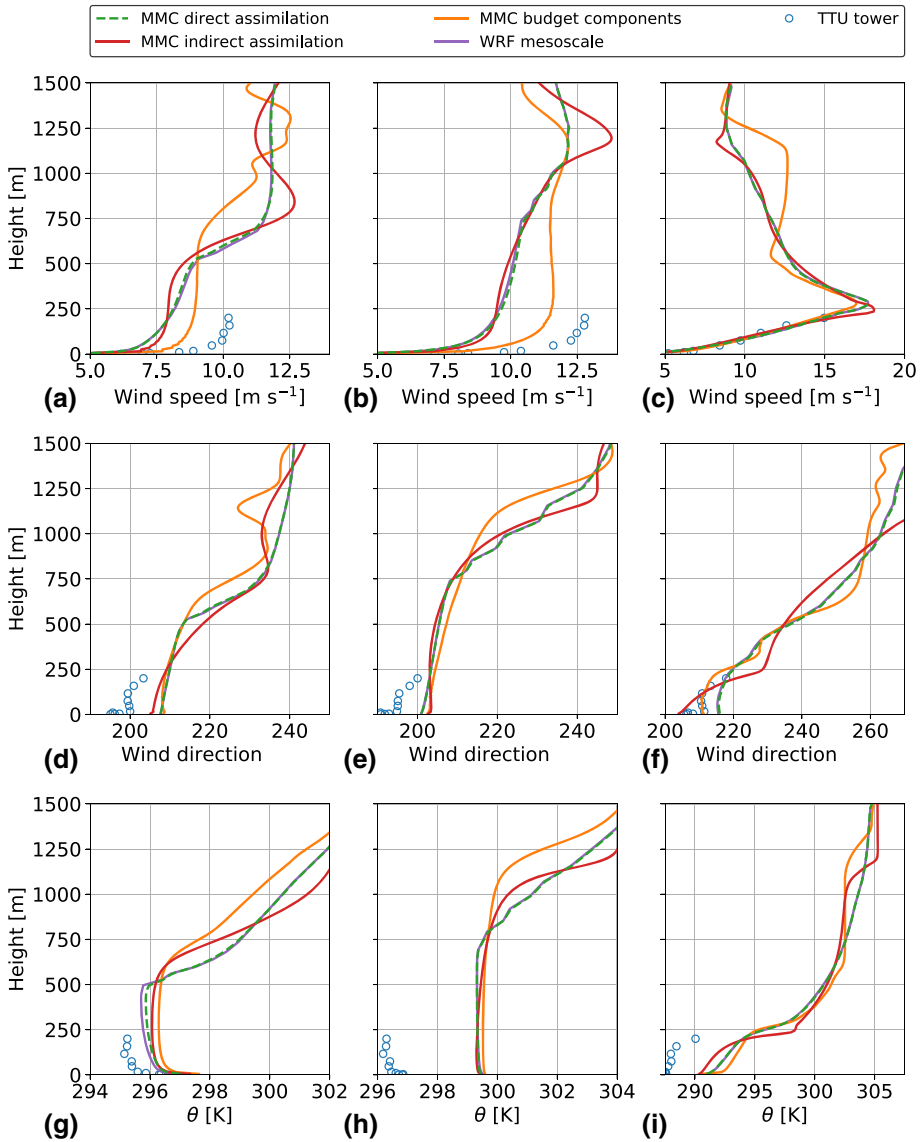
Fig. 5 Vertical profiles of **a–c** horizontal wind speed, **d–f** wind direction, and **g–i** virtual potential temperature, averaged over 1 h, starting at (left panel) 1800 UTC, (middle panel) 2200 UTC, and (right panel) 0600 UTC. Direct and indirect data assimilation are compared with TTU tower observations, WRF mesoscale data, and MMC using budget components. The microscale results represent planar-averaged data

4.3 Turbulence Statistics

The time history of TKE at 80 m and its vertical distribution for three particular times of the day are shown in Figs. 1 and 6, respectively. As already noted in Sect. 2.2.1, direct data assimilation leads to a severe overprediction of TKE during convective and neutral conditions. By contrast, applying indirect data assimilation brings the TKE back to more
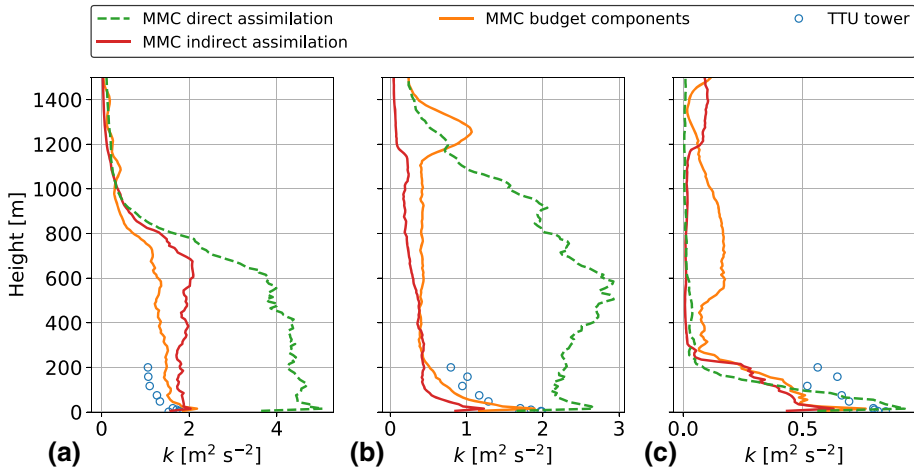
Fig. 6 Vertical profiles of TKE (k), averaged over 1 h, starting at **a** 1800 UTC, **b** 2200 UTC, and **c** 0600 UTC. Direct and indirect data assimilation are compared with TTU tower observations and MMC using budget components. The microscale data are obtained from a single virtual tower

realistic values. During neutral and stable conditions, indirect assimilation results agree with tower observations and the budget components approach. For convective conditions in Fig. 6a, the TKE predicted by indirect data assimilation is slightly higher than both MMC budget components results and TTU observations.

Turbulence spectra of horizontal and vertical wind speed at 80 m for different times of the day are shown in Fig. 7. The spectra are computed from 1 h of data with Welch's method (using 10-min segments and a Hanning window function). As expected, direct data assimilation overpredicts the TKE during both convective and neutral conditions. Indirect data assimilation, on the other hand, agrees well with MMC via budget components during the various stability conditions. Moreover, the spectra computed from results of both approaches compare well with the observed turbulence spectra, showing that indirect data assimilation does not alter the turbulence energy cascade.

4.4 Discussion

The unphysically high levels of TKE predicted by direct data assimilation can be traced back to the process of turbulence production by means of shear and buoyancy. Upon closer inspection of Fig. 5a, the WRF mesoscale velocity profiles and therefore the microscale profiles of the direct data assimilation case have greater vertical shear than the budget components case, leading to an increased production of turbulence. Normally, the higher levels of turbulence will increase vertical transport of momentum, which in turn will reduce the velocity shear, hence the production of turbulence. However, the direct data assimilation algorithm (Eq. 4) effectively adapts the external forcing so as to counteract any change in vertical transport of momentum, thereby maintaining the high and unrealistic shear in the velocity profile, and decoupling mean velocity profiles and turbulent mixing. A similar problem arises with the virtual-potential-temperature profile and the production of turbulence caused by buoyancy. Superadiabatic profiles during the daytime in Fig. 5g produce too much buoyancy production, but the nature of direct data assimilation prevents the enhanced vertical turbulent
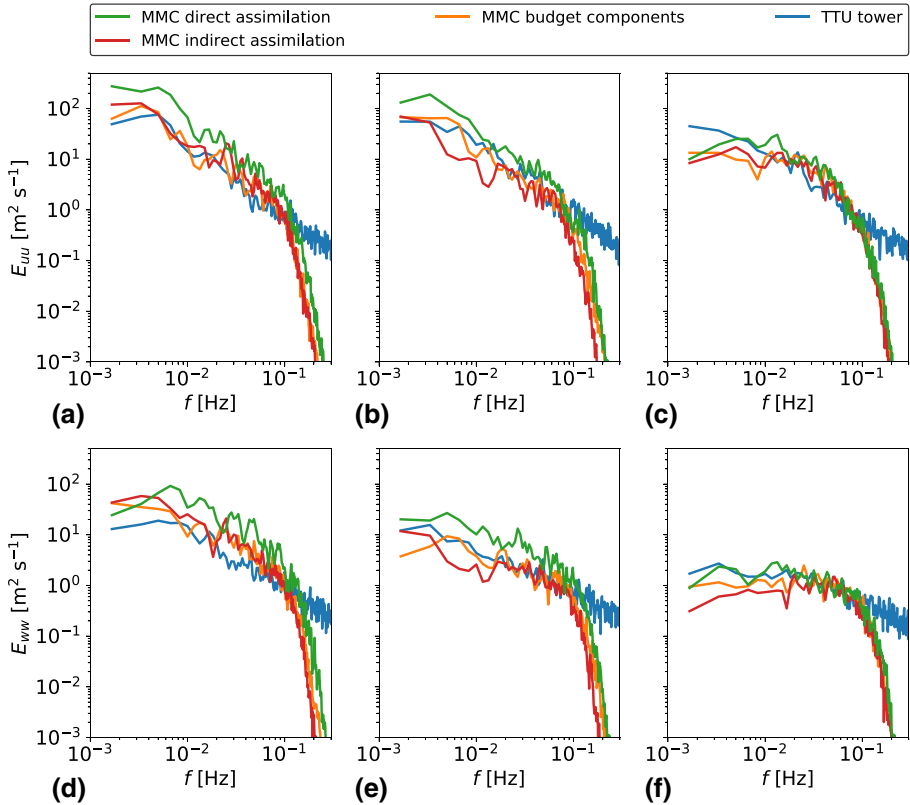
Fig. 7 Turbulence spectra of **a–c** horizontal wind speed and **d–f** vertical wind speed at 80 m, using 1 h of data starting at (left panel) 1800 UTC, (middle panel) 2200 UTC, and (right panel) 0600 UTC. Results of MMC via budget components (i.e., simulation *w0_L0* of D2020) and improved profile assimilation (Sect. 2.2.2) are compared with observations from the TTU tower

heat flux from decreasing the superadiabatic temperature gradients. Buoyancy production is particularly sensitive to the virtual-potential-temperature profile, because even the slightest difference in lapse rate can lead to large differences in turbulence intensity.

Failure of the direct data assimilation approach can be attributed to, (1) inaccuracy of the mesoscale profiles, and (2) the inability of the forcing term algorithm to cope with such inaccuracies. The reason why mesoscale profiles of wind speed and temperature cannot be directly used to drive microscale simulations is because the profile shape is, to a large extent, dictated by the representation of turbulence in the respective numerical model. In the mesoscale solver, the effect of turbulence is completely modeled by the ABL parametrization scheme, which attempts to reduce all the turbulent processes into one or more fairly simple equations. On the other hand, the LES should arguably produce a more accurate turbulence profile through the boundary layer than an ABL scheme because most energy-containing turbulent structures are resolved. Consequently, the shapes of the wind-speed and virtual-potential-temperature profiles predicted by the mesoscale model are not necessarily consistent with the microscale representation of turbulence. A successful and robust mesoscale-to-LES assimilation methodology should therefore allow the LES to find its own equilibrium between

mean profiles, turbulence production, and turbulent mixing, even if this means deviating from the mesoscale profiles.

Direct data assimilation, however, does not account for possible errors in the mesoscale profiles, and the lack of correlation in space and time in the forcing term algorithm results in too much variability of the predicted source terms (e.g., Fig. 3d), which facilitates the suppression of mean-profile corrections by turbulent mixing. Restricting the algorithm's control capacity by simply decreasing the controller gain or applying proportional-integral control turns out not to be sufficient and still leads to unphysically high turbulence intensity. Indirect data assimilation, on the other hand, allows turbulence to correct the boundary-layer profiles when necessary, while still following the overall mesoscale trends. For example, in the daytime profiles of Fig. 5 (left panels), the wind shear and virtual-potential-temperature gradient in the indirect assimilation case are lower than the WRF mesoscale data and match better with the gradients from the MMC budget components solution, which then results in more realistic TKE values in Fig. 6a. At night, the WRF model yields a good prediction of the low-level jet that does not need to be corrected, so the microscale results follow the mesoscale input profiles in Fig. 5 (right panels).

5 Conclusion

We have described the development of a new mesoscale-to-microscale coupling technique for horizontally homogeneous microscale flow conditions by means of internal forcing, as opposed to forcing via boundary conditions. Traditional internal forcing approaches directly apply mesoscale momentum and temperature-transport-equation source terms—neither default outputs of most mesoscale solvers nor easily measured quantities in the field—to the microscale transport equations. In contrast, the proposed profile assimilation technique estimates these mesoscale source terms based on mesoscale time–height profiles of wind speed and virtual potential temperature, quantities that are more commonly available and can be relatively easily measured in the field. Two different algorithms were proposed, and the performance of these algorithms was compared with the standard budget components approach, meteorological tower observations, and WRF mesoscale simulations for a typical diurnal cycle over the SWiFT site in Texas. The proposed data assimilation techniques admittedly remove physics-based mesoscale-influence terms from the microscale governing equations and replace them with estimates of these terms derived using basic control theory. However, we feel this to be a completely viable approach when the physical mesoscale source terms are simply unavailable.

An intuitive direct data assimilation algorithm for estimating the mesoscale source terms was shown to produce reasonable results in terms of mean-flow quantities. However, the simple algorithm also leads to unphysically high levels of shear and turbulence; therefore, it is not suitable for MMC applications such as wind energy, where shear and turbulence are the main drivers of wind-turbine fatigue. The underlying reason for the algorithm's failure was its inability to cope with possible inaccuracies in the mesoscale profiles, caused by differences in the representation of turbulence in mesoscale and microscale solvers.

Based on lessons learned from the intuitive direct data assimilation forcing algorithm, a modified algorithm accounting for vertical coherence in the mesoscale source terms was developed. Comparing the simulation results with the traditional budget components approach showed that the new algorithm can handle inaccuracies in mesoscale profiles and allows LES to realistically capture interactions between the mesoscale and microscale pro-

cesses. With the new algorithm, wind shear and virtual-potential-temperature gradients are correctly resolved, thereby leading to more accurate predictions of turbulence statistics. This finding also revealed the underlying responsibilities of the mesoscale and microscale solvers in an MMC framework: the mean-flow trends are dictated by the mesoscale simulation, and one cannot expect the microscale solver to correct for large biases in mean-flow quantities or inaccurate timing of large-scale events. The added value of coupling to a microscale solver is that the latter improves the prediction of wind shear and turbulence statistics inside the boundary layer, even in relatively simple conditions of flat terrain and a simple diurnal cycle.

Herein, we only used the profile assimilation technique to couple microscale LES with WRF simulations. However, as the proposed technique requires just the time–height profiles of velocity and virtual potential temperature, microscale simulations could also be driven by observational data, and this is the subject of further research. Furthermore, vertical coherence was introduced into the forcing algorithm as a simple polynomial fit to the vertical error profile. However, using higher-order polynomials resulted in a runaway near the edges of the profiles. Future research is needed to improve the profile assimilation approach by investigating more advanced controllers, based on algorithms like extended Kalman filtering, or by using more complex shape functions that more adequately represent the vertical structure of mesoscale source terms.

References

Andren A, Brown AR, Mason PJ, Graf J, Schumann U, Moeng CH, Nieuwstadt FTM (1994) Large-eddy simulation of a neutrally stratified boundary layer: a comparison of four computer codes. Q J R Meteorol Soc 120(520):1457–1484. https://doi.org/10.1002/qj.49712052003

Baas P, Bosveld FC, Lenderink G, van Meijgaard E, Holtslag AAM (2010) How to design single-column model experiments for comparison with observed nocturnal low-level jets. Q J R Meteorol Soc 136(648):671–684. https://doi.org/10.1002/qj.592

Baklanov AA, Nuterman RB (2009) Multi-scale atmospheric environment modelling for urban areas. Adv Sci Res 3(1):53–57. https://doi.org/10.5194/asr-3-53-2009

Basu S, Porté-Agel F (2006) Large-eddy simulation of stably stratified atmospheric boundary layer turbulence: a scale-dependent dynamic modeling approach. J Atmos Sci 63(8):2074–2091. https://doi.org/10.1175/JAS3734.1

Basu S, Vinuesa JF, Swift A (2008) Dynamic LES modeling of a diurnal cycle. J Appl Meteorol Clim 47(4):1156–1174. https://doi.org/10.1175/2007JAMC1677.1

Beare RJ, Macvean MK, Holtslag AAM, Cuxart J, Esau I, Golaz JC, Jimenez MA, Khairoutdinov M, Kosović B, Lewellen D, Lund TS, Lundquist JK, Mccabe A, Moene AF, Noh Y, Raasch S, Sullivan PP (2006) An intercomparison of large-eddy simulations of the stable boundary layer. Boundary-Layer Meteorol 118(2):247–272. https://doi.org/10.1007/s10546-004-2820-6

Bosveld FC, Baas P, van Meijgaard E, de Bruijn EIF, Steeneveld GJ, Holtslag AAM (2014) The third GABLS intercomparison case for evaluation studies of boundary-layer models. Part A: case selection and set-up. Boundary-Layer Meteorol 152(2):133–156. https://doi.org/10.1007/s10546-014-9917-3

Churchfield MJ, Lee S, Michalakes J, Moriarty PJ (2012a) A numerical study of the effects of atmospheric and wake turbulence on wind turbine dynamics. J Turbul 13(14):1–32. https://doi.org/10.1080/14685248.2012.668191

Churchfield MJ, Lee S, Moriarty PJ, Martinez LA, Leonardi S, Vijayakumar G, Brasseur J (2012b) A large-eddy simulation of wind-plant aerodynamics. In: Proceedings of 50th AIAA aerospace sciences meeting including the new horizons forum and aerospace exposition

Draxl C, Allaerts D, Quon E, Churchfield MJ (2020) On the averaging of mesoscale budget components for mesoscale-to-microscale coupling. Boundary-Layer Meteorol (in press)

Duynkerke PG, de Roode SR, van Zanten MC, Calvo J, Cuxart J, Cheinet S, Chlond A, Grenier H, Jonker PJ, Köhler M, Lenderink G, Lewellen D, Lappen C, Lock AP, Moeng CH, Müller F, Olmeda D, Piriou JM, Sánchez E, Sednev I (2004) Observations and numerical simulations of the diurnal cycle of the EUROCS stratocumulus case. Q J R Meteorol Soc 130(604):3269–3296. https://doi.org/10.1256/qj.03.139

Esau IN (2004) Simulation of Ekman boundary layers by large eddy model with dynamic mixed subfilter closure. Environ Fluid Mech 4(3):273–303. https://doi.org/10.1023/B:EFMC.0000024236.38450.8d

Gibbs JA, Fedorovich E (2016) Sensitivity of turbulence statistics in the lower portion of a numerically simulated stable boundary layer to parameters of the Deardorff subgrid turbulence model. Q J R Meteorol Soc 142(698):2205–2213. https://doi.org/10.1002/qj.2818

Gibbs JA, Fedorovich E, van Eijk AMJ (2011) Evaluating weather research and forecasting (WRF) model predictions of turbulent flow parameters in a dry convective boundary layer. J Appl Meteorol Climatol 50(12):2429–2444. https://doi.org/10.1175/2011JAMC2661.1

Grötzbach G (1987) Direct numerical and large eddy simulation of turbulent channel flows. Encycl Fluid Mech 6:1337–1391

Haupt SE, Kotamarthi R, Feng Y, Mirocha JD, Koo E, Linn R, Kosović B, Brown B, Anderson A, Churchfield MJ, Draxl C, Quon E, Shaw W, Berg L, Rai R, Ennis BL (2017) Second year report of the atmosphere to electrons mesoscale to microscale coupling project: nonstationary modeling techniques and assessment. Pacific Northwest National Laboratory, Richland, WA, Technical Report PNNL-26267

Heinze R, Moseley C, Böske LN, Muppa SK, Maurer V, Raasch S, Stevens B (2017) Evaluation of large-eddy simulations forced with mesoscale model output for a multi-week period during a measurement campaign. Atmos Chem Phys 17(11):7083–7109. https://doi.org/10.5194/acp-17-7083-2017

Hirth B, Schroeder J (2014) A summary of the National Wind Institute meteorological measurement facilities at the Texas Tech University's Reese Technology Center field site. Texas Tech University, Technical report

Kelley CL, Ennis BL (2016) SWiFT site atmospheric characterization. Sandia National Laboratories, Albuquerque, NM, Technical Report SAND2016-2016

Kleissl J, Kumar V, Meneveau C, Parlange MB (2006) Numerical study of dynamic smagorinsky models in large-eddy simulation of the atmospheric boundary layer: validation in stable and unstable conditions. Water Resour Res. https://doi.org/10.1029/2005WR004685

Kosović B (1997) Subgrid-scale modelling for the large-eddy simulation of high-Reynolds-number boundary layers. J Fluid Mech 336:151–182. https://doi.org/10.1017/S0022112096004697

Kosović B, Curry JA (2000) A large eddy simulation study of a quasi-steady, stably stratified atmospheric boundary layer. J Atmos Sci 57(8):1052–1068. https://doi.org/10.1175/1520-0469(2000)057<1052:ALESSO>2.0.CO;2

Kumar V, Kleissl J, Meneveau C, Parlange MB (2006) Large-eddy simulation of a diurnal cycle of the atmospheric boundary layer: atmospheric stability and scaling issues. Water Resour Res 42(6):1–18

Kumar V, Svensson G, Holtslag AAM, Meneveau C, Parlange MB (2010) Impact of surface flux formulations and geostrophic forcing on large-eddy simulations of diurnal atmospheric boundary layer flow. J Appl Meteorol Clim 49(7):1496–1516. https://doi.org/10.1175/2010JAMC2145.1

Lin CL, McWilliams JC, Moeng CH, Sullivan PP (1996) Coherent structures and dynamics in a neutrally stratified planetary boundary layer flow. Phys Fluids 8(10):2626–2639. https://doi.org/10.1063/1.869048

Liu YS, Miao SG, Zhang CL, Cui GX, Zhang ZS (2012) Study on micro-atmospheric environment by coupling large eddy simulation with mesoscale model. J Wind Eng Ind Aerodyn 107–108:106–117. https://doi.org/10.1016/j.jweia.2012.03.033

Mandel J, Beezley JD, Kochanski AK (2011) Coupled atmosphere-wildland fire modeling with WRF 3.3 and SFIRE 2011. Geosci Model Dev 4(3):591–610. https://doi.org/10.5194/gmd-4-591-2011

Mason PJ (1989) Large-eddy simulation of the convective atmospheric boundary layer. J Atmos Sci 46(11):1492–1516. https://doi.org/10.1175/1520-0469(1989)046<1492:LESOTC>2.0.CO;2

Mason PJ, Derbyshire SH (1990) Large-eddy simulation of the stably-stratified atmospheric boundary layer. Boundary-Layer Meteorol 53(1–2):117–162. https://doi.org/10.1007/BF00122467

Mason PJ, Thomson DJ (1987) Large-eddy simulations of the neutral-static-stability planetary boundary layer. Q J R Meteorol Soc 113(476):413–443. https://doi.org/10.1002/qj.49711347602

Mirocha J, Kosović B, Kirkil G (2014) Resolved turbulence characteristics in large-eddy simulations nested within mesoscale simulations using the weather research and forecasting model. Mon Weather Rev 142(2):806–831. https://doi.org/10.1175/MWR-D-13-00064.1

Moeng CH (1984) A large-eddy-simulation model for the study of planetary boundary-layer turbulence. J Atmos Sci 41(13):2052–2062. https://doi.org/10.1175/1520-0469(1984)041<2052:ALESMF>2.0.CO;2

Moeng CH, Sullivan PP (1994) A comparison of shear- and buoyancy-driven planetary boundary layer flows. J Atmos Sci 51(7):999–1022

Muñoz-Esparza D, Kosović B (2018) Generation of inflow turbulence in large-eddy simulations of nonneutral atmospheric boundary layers with the cell perturbation method. Mon Weather Rev 146(6):1889–1909. https://doi.org/10.1175/MWR-D-18-0077.1

Muñoz-Esparza D, Kosović B, van Beeck J, Mirocha J (2015) A stochastic perturbation method to generate inflow turbulence in large-eddy simulation models: application to neutrally stratified atmospheric boundary layers. Phys Fluids 27(3):035–102. https://doi.org/10.1063/1.4913572

Nakayama H, Takemi T, Nagai H (2015) Large-eddy simulation of turbulent winds during the Fukushima Daiichi Nuclear Power Plant accident by coupling with a meso-scale meteorological simulation model. Adv Sci Res 12(1):127–133. https://doi.org/10.5194/asr-12-127-2015

Neggers RAJ, Siebesma AP, Heus T (2012) Continuous single-column model evaluation at a permanent meteorological supersite. Bull Am Meteorol Soc 93(9):1389–1400. https://doi.org/10.1175/BAMS-D-11-00162.1

Nieuwstadt FTM, Mason PJ, Moeng CH, Schumann U (1993) Large-eddy simulation of the convective boundary layer: a comparison of four computer codes. Turbul Shear Flows 8:343–367

Olsen BT (2018) Mesoscale to microscale coupling for determining site conditions in complex terrain. Ph.D. thesis, Technical University of Denmark

Pedersen JG, Gryning SE, Kelly M (2014) On the structure and adjustment of inversion-capped neutral atmospheric boundary-layer flows: large-eddy simulation study. Boundary-Layer Meteorol 153(1):43–62. https://doi.org/10.1007/s10546-014-9937-z

Quon EW, Ghate AS, Lele SK (2018) Enrichment methods for inflow turbulence generation in the atmospheric boundary layer. J Phys Conf Ser 1037(072):054. https://doi.org/10.1088/1742-6596/1037/7/072054

Saiki EM, Moeng CH, Sullivan PP (2000) Large-eddy simulation of the stably stratified planetary boundary layer. Boundary-Layer Meteorol 95(1):1–30. https://doi.org/10.1023/A:1002428223156

Sanz Rodrigo J, Chávez Arroyo RA, Moriarty P, Churchfield MJ, Kosović B, Réthoré PE, Hansen KS, Hahmann A, Mirocha FD, Rife D (2017a) Mesoscale to microscale wind farm flow modeling and evaluation. WIREs Energy Environ 6:e214

Sanz Rodrigo J, Churchfield MJ, Kosović B (2017b) A methodology for the design and testing of atmospheric boundary layer models for wind energy applications. Wind Energy Sci 2:35–54

Schalkwijk J, Jonker HJJ, Siebesma AP, Bosveld FC (2015) A year-long large-eddy simulation of the weather over Cabauw: an overview. Mon Wea Rev 143(3):828–844. https://doi.org/10.1175/MWR-D-14-00293.1

Schumann U (1975) Subgrid scale model for finite difference simulations of turbulent flows in plane channels and annuli. J Comput Phys 18(4):376–404. https://doi.org/10.1016/0021-9991(75)90093-5

Skamarock WC, Klemp J, Dudhia J, Gill DO, Barker D, Wang W, Powers JG (2008) A description of the advanced research WRF version 3. National Center for Atmospheric Research, Boulder, CO, Technical Report NCAR/TN-475+STR

Stauffer DR, Seaman NL (1994) Multiscale four-dimensional data assimilation. J Appl Meteorol 33(3):416–434. https://doi.org/10.1175/1520-0450(1994)033<0416:MFDDA>2.0.CO;2

Vionnet V, Martin E, Masson V, Lac C, Naaim Bouvet F, Guyomarc'h G (2017) High-resolution large eddy simulation of snow accumulation in alpine terrain. J Geophys Res Atmos 122(20):11,005–11,021. https://doi.org/10.1002/2017JD026947

Publisher's Note Springer Nature remains neutral with regard to jurisdictional claims in published maps and institutional affiliations.